

Low temperature processed efficient and stable perovskite solar cell

Ashraf Uddin*, Md Arafat Mahmud, Naveen Kumar Elumalai, Mushfika Baishakhi Upama, Dian Wang, Faiazul Haque, Cheng Xu

School of Photovoltaic and Renewable Energy Engineering, University of New South Wales, Sydney, NSW 2052, Australia

*Corresponding author: E-mail: a.uddin@unsw.edu.au

DOI: 10.5185/amlett.2019.2050
www.vbripress.com/aml

Abstract

MA_{0.6}FA_{0.4}PbI₃ material based efficient and stable perovskite solar cells (PSCs) are fabricated by electron transport layer (ETL) interfacial modification. The highest power conversion efficiency (PCE) of device was ~ 17%. Cesium acetate and cesium carbonate were used with low temperature processed sol-gel ZnO ETL for interface modifications. Low leakage current and enhanced dark injection current are observed from dark current – voltage measurement. From the electrochemical impedance spectroscopy (EIS) measurement higher recombination resistance and lower interfacial contact resistance are observed in the PSC devices. Mott-Schottky analysis also shows the higher flat-band potential and enhanced device performance with cesium acetate ETL. Cesium acetate related ZnO ETL has large grain size which leads to reduce the device series resistance and contact resistance in PSC compared to cesium carbonate ETL related device. Perovskite film on cesium acetate ETL has better surface morphology, topography and hydrophobicity characterization compared to perovskite film grown on cesium carbonate ETL film. The material work function and electron injection barrier are also investigated by X-Ray photoelectron spectroscopy (XPS) measurement and ultraviolet photoelectron spectroscopy (UPS). From electrochemical impedance spectroscopy measurements the charge transport behaviour and trap-assisted carrier recombination are estimated. Fabricated PSCs device stability has been measured for a month-long degradation study. The PSC device stability is observed four times higher with cesium acetate PSCs compared to cesium carbonate ETL related PSCs. The overall device PCE is around 82% higher with cesium acetate compared to cesium carbonate devices. Copyright © 2019 VBRI Press.

Keywords: Solar cells, perovskite solar cells, efficiency, stability, ZnO.

Introduction

Methyl ammonium lead halide (CH₃NH₃PbX₃) perovskite solar cells (PSCs) have shown tremendous potentials for low cost electric power generation; [16, 25, 32, 61, 76] where X is denoted as an individual halogen element [11, 38, 41, 74, 79] (iodine (I), chlorine (Cl), and bromine (Br)) or a composition [15, 64, 67, 76, 83, 87] of them with a fixed molar ratio. Methyl ammonium lead triiodide (CH₃NH₃PbI₃) has a direct band gap of 1.57 eV [8] and it is also blessed with high carrier mobility of 10 cm² V⁻¹ s⁻¹ [75], large exciton diffusion length of ~1 μm [67] and exciton binding energy ~16 meV [56]. Perovskite solar cells do not require any heterojunction band-edge offset barrier for the dissociation of excitons [14] like organic solar cells. Electron transport layer (ETL) plays an important role in PSCs for contact selectivity [26] and the device performance [33, 42]. ETL works as electron extractor to one side of the device and blocks the hole transporting from another side of device in PSC [26]. ETL is also play an important role to improve the device performance by enhancing the fill factor [33]

and the open circuit voltage [42]. The perovskite/ETL interface quality can be control by optimising the perovskite layer and ETL surface morphology [84]. The compact TiO₂ layer as ETL is used in most of the highly efficient PSCs which need a high temperature sintering process of ~500 °C [7, 11, 30, 43, 76]. One of the fundamental barriers to mass production of PSCs on flexible substrates by roll-to-roll process is the high temperature (~500 °C) processing of TiO₂ [28, 69]. The optimum temperature range for the flexible substrate is within 100-150 °C [39]. So it is important to replace the high temperature processed TiO₂ ETL with a low temperature alternative for large scale production of PSCs. Zinc Oxide (ZnO) is a wide band gap semiconductor material with similar identical electrical affinity as TiO₂ [84]. ZnO film can be deposited at low temperature (< 150 °C) process with high structural quality [58, 59]. It has several orders of higher electrical conductivity compared to TiO₂ [40, 45]. Low temperature processed sol-gel ZnO film can be a promising alternative for ETL for the PSCs for commercial applications.

In the previous work we have reported the low temperature processed sol-gel ZnO as ETL for perovskite solar cells [24]. However, owing to the chemisorption of oxygen, sol-gel ZnO ETL contains energetic disorder induced trap states [46, 54, 65]. The electron transport hopping phenomena in these trap states lead to carrier recombination [38, 46, 49, 52]. This is a major issue in low temperature processed sol-gel ZnO ETL. To address this, an additional ETL PCBM ([6, 6]-phenyl C61 butyric acid methyl ester) was inserted as an intermediate layer in between the low temperature processed ZnO layer and perovskite layer for the trap-state passivation [29, 52, 85].

The PCBM buffer layer atop ZnO film [38] has been reported to diffuse during the 100 deg. C annealing session of perovskite film [12]. Normally, the PCE of PSCs with ZnO/PCBM double layer ETL is relatively low (highest reported PCE is ~12.20%) [38]. The short circuit current J_{sc} of PSCs is relatively lower with Al doped ZnO (AZO) ETL compared to pristine ZnO ETL based PSCs [52, 85]. The surface modification of ZnO with cesium acetate (acetate) shown superior conductive property in organic solar cells compared to pristine ZnO film [1]. But until there is no report on PSCs with cesium acetate doped ZnO as ETL. It is an important investigation for perovskite solar cells to understand the effect of bulk modification of ZnO along with cesium based dopants. The effect on the charge transport property [22, 51, 60], hysteresis and device degradation phenomena [73] are important parameters to understand for ZnO ETL based devices. In this work we have tried to find out these effects.

In the current study, we have fabricated highly efficient MA_{0.6}FA_{0.4}PbI₃ based PSCs along with sol-gel ZnO ETL, doped with cesium compounds (acetate and carbonate). The PSCs device performance, hysteresis and degradation phenomena are investigated systematically and compared. Improve device performance is observed with acetate doped ZnO ETL. Material work function, surface topography and electron transport barrier are investigated with structural, optical and electrochemical characterizations. The fabricated PSC device stability has also been conducted for a period of one month to understand the device stability.

Experimental details

Device Fabrication

Patterned ITO/glass substrates were cleaned sequentially with Hellmanex III, DI water, Acetone and Isopropanol with duration of 10 minutes for each. For ZnO/carbonate ETL, 0.48 M sol-gel ZnO solution was prepared by dissolving zinc acetate dihydrate in 2-Methoxyethanol with an additive ethanolamine and by vigorous stirring for 24 hours. ZnO solution was spin coated on ITO surface on glass substrate at 4000 rpm for 60 seconds. ZnO film was annealed at normal atmosphere on a hotplate at 140 °C for 30 minutes.

After that 0.5 wt% carbonate solution in DI water was spin-coated on ZnO film for 30 seconds at 3000 rpm and dried at 100 °C for about two hours. We have repeated the process as it is demonstrated in the perovskite solar cell literature for TiO₂ ETL [82]. We have denoted the ZnO/Cs carbonate double layer ETL as carbonate ETL for reference in this manuscript. A 0.09 M cesium acetate solution in 2-methoxyethanol was prepared by stirring for 4 hours at a temperature of 80°C for acetate ETL. 0.48 M sol-gel ZnO solution was separately doped with cesium acetate solution to get 5 different solution concentrations of 0, 1, 2, 3, 4 and 5 wt%. The mixed organic cation based perovskite (MA_{0.6}FA_{0.4}PbI₃) precursor solution was prepared using PbI₂ (1 M), MAI (0.6 M) and FAI (0.4 M) powder in anhydrous DMF (*N, N*-dimethylformamide) solvent and the solution was stirred at 70 °C for 24 hours for both the acetate and carbonate ETL devices. The perovskite film was fabricated in gas-quenching method [27, 48]. After that the perovskite film was annealed at 100 °C for 10 minutes in restricted volume solvent annealing (RVSA) method in nitrogen environment. For HTL, 73.3 mg/ml Spiro-OMeTAD solution in chlorobenzene was doped with 17.5 μL Li-TFSI (520 mg/ml in Acetonitrile) and 28.8 μL 4-TBP for hole transport layer (HTL). The Spiro-OMeTAD layer was spin coated with 3000 rpm for 30 seconds on the perovskite film. Finally, a 100 nm thick Ag layer was deposited by thermal evaporation with an evaporation rate of 2 Å/s under a vacuum condition of 1x10⁻⁶ mbar on the HTL to complete the device structure. The active device area was around 4.5 mm² with the use of a metal mask. The layer configurations of the devices were: ITO/ZnO/acetate or carbonate ETL/MA_{0.6}FA_{0.4}PbI₃ perovskite/Spiro-OMeTAD/Ag.

Device characterization

A NREL calibrated Keithley 2400 Source meter under 100 mW/cm² (one sun at AM 1.5G) was used for the current-voltage characteristic measurements of PSC devices. A non-reflective aperture (4.5 mm²) mask was used over the cells during IV measurement. A Perkin Elmer-Lambda 950 machine was used for optical characterization such as optical transmittance, reflectance and absorbance measurement. XRD measurement was performed with 0.02° angular step size. The surface roughness was measured with Bruker Dimension ICON SPM AFM machine. Surface topography was characterized by Carl Zeiss AURIGA Cross Beam SEM. Ramé-hart contact angle goniometer (Model 200) was used for the contact angle measurement. Using DROP-image advanced software the contact angles were precisely determined. ESacetateLAB250Xi instrument was used to conduct the XPS and UPS characterization. An Autolab PGSTAT-30 equipped was used for the impedance analysis with a frequency range from 1 MHz to 1 Hz. The linearity of the response oscillating amplitude was as low as 20 mV (RMS).

Results and discussion

The XPS spectra of carbonate and acetate ETL are shown in **Fig. 1(A)** and **1(B)** with demonstrating elemental peaks. The information pertaining to the elemental analysis of carbonate and acetate ETL films from XPS characterization are listed in **Table 1**. Both the carbonate and acetate ETL films exhibit Cs_{3d} and Zn_{2p} spectra as shown in **Fig. 1(A)** [37]. This is confirmed the successful doping of Cs atoms in both carbonate and acetate ZnO ETL films by spin deposition method. The atomic percentage of cesium is relatively higher in carbonate ETL (6.5%) than in acetate ETL film (2.3%). The Cs_{3d} XPS peak in acetate ETL moves to larger binding energy than carbonate ETL. This indicate that the oxidation state of Cs_{3d} peak in acetate ETL is higher [78]. Higher concentration of donor electrons can facilitate the injection [9, 78] of electrons into the ZnO lattice. We have also conducted UPS measurement of carbonate and acetate ETLs along with pure ZnO film on ITO/glass substrate. **Fig. 1(B)** shows the UPS curves for pure ZnO, carbonate ETL and acetate ETL films. The estimated work functions of pure ZnO film, carbonate ETL and acetate ETL are 3.84 eV, 3.80 eV and 3.75 eV. The reduction of work function for both carbonate and acetate ETLs can be attributed to the donor electrons from cesium atom compared to pristine ZnO film [37]. It denotes that the vacancies in pure ZnO film [37, 78] are passivated by donor electrons. The Fermi position is upshifted in Cs doped ZnO compared to pure ZnO ETL. The Fermi level of acetate ETL is also upshifted by 50 meV, relative to carbonate film. This denotes enhanced n-type property [37] of acetate ETL film. Cs atom can take place in the interstitial positions of ZnO lattice. The interstitial Cs atoms in ZnO matrix donate electrons to enhance the n-type property of ZnO ETL [37]. On the other hand, when the dopant concentration is very high, the dominance of acceptor states can lower down the n-type conductivity of ZnO film [86]. Thus, Fermi-level of carbonate ETL demonstrates downward shift, compared to acetate ETL (**Fig. 1(B)**).

The peak width or full width at half maximum (FWHM), normalized peak intensity, and crystallite size of acetate and carbonate films are calculated from the Debye Scherrer equation [57]. **Fig. 1(C)** shows the crystallite dimension of the ETL films for qualitative comparison. Both the both acetate and carbonate ETL films demonstrate (002) characteristic peaks [68].

Table 1. Start, peak and end binding energy of elemental peaks, full width at half maximum (FWHM) and atomic percentage of carbonate and acetate ETL film are calculated from the spectral fitting of X-Ray photoelectron spectroscopy (XPS) data.

Peak	Start Binding Energy (eV)		Peak Binding Energy (eV)		End Binding Energy (eV)		Full Width at Half Maximum (FWHM) (eV)		Atomic Percentage (%)	
	Acetate	Carbonate	Acetate	Carbonate	Acetate	Carbonate	Acetate	Carbonate	Acetate	Carbonate
C_{1s}	298	298	284.83	284.68	280.59	275.19	2.52	2.59	10.94	16.11
O_{1s}	537.69	545	530.08	526.8	525.49	519.51	3.13	2.98	45.24	45.37
Cs_{3d}	742	742	724.34	719.96	716	712.6	2.51	2.49	2.3	6.47
Zn_{2p}	1049.56	1047.69	1020.97	1016.93	1016.27	1009.89	2.58	2.71	41.52	26.11

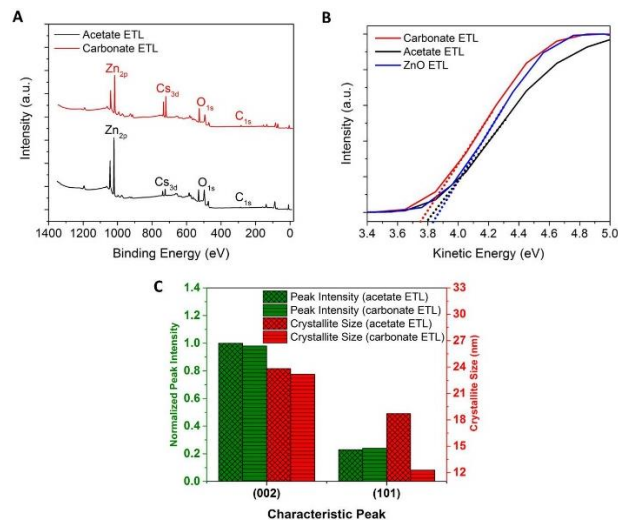


Fig. 1. (A) The elemental peaks from the X-Ray photoelectron spectroscopy (XPS) survey spectra of carbonate ETL and acetate ETL on ITO/glass substrate; (B) Evolution of secondary electron edge for pure ZnO, carbonate and acetate doped ZnO ETL film from ultraviolet photoelectron spectroscopy (UPS) measurement; (C) Normalized peak intensity and crystallite size of perovskite film on acetate and carbonate ETL from XRD spectral fitting.

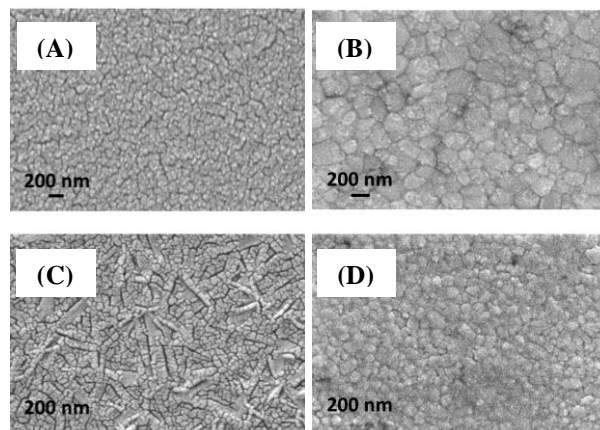


Fig. 2. Top view Scanning Electron Microscopy (SEM) images of (A) acetate and (C) carbonate ETL films, $MA_{0.6}FA_{0.4}PbI_3$ perovskite film on top of (B) acetate ETL film and (D) carbonate ETL film.

The surface morphology of both the ETL films was investigated with SEM imaging (**Fig. 2**). As observed from **Fig. 2(A)** and **2(C)**, the grains are more closely packed in acetate film with reference to carbonate films. The random distribution of pin-hole induced surface morphology with carbonate ETL film conforms to the previous report by Ma *et al.* [44]. It has also been demonstrated that excess alkaline dopant (Na in their

case) can induce small pores and dislocation crack in doped ZnO film [44]. The difference in grain distribution between carbonate and acetate films is also consistent with the respective AFM characterization. The root mean square (RMS) surface roughness of carbonate ETL film (17.90 nm) is significantly higher than acetate ETL film (10.80 nm).

The SEM images of MA_{0.6}FA_{0.4}PbI₃ perovskite films on top of acetate and carbonate ETL films are shown in Fig. 2(B) and 2(D), respectively. The perovskite grain size on acetate ETL is comparatively large than same on carbonate ETL. Growth of larger grain-sized perovskite film is contributed by the void-free, favourable surface topography and morphology of the acetate ETL film underneath [5].

We have also conducted AFM imaging of identically fabricated perovskite films atop both the ETL films. Perovskite on carbonate ETL demonstrates about 10.5% higher average surface roughnesses (16.90 nm) than the same on acetate ETL (15.30 nm). The heightened surface roughness atop carbonate ETL conforms to the inferior surface morphology and topography of carbonate ETL.

Device performance

Perovskite solar cells with acetate and carbonate ETL films have been fabricated and investigated. The PSC device configuration was: ITO/acetate or carbonate ETL/MA_{0.6}FA_{0.4}PbI₃ perovskite /Spiro-OMeTAD/Ag as shown in Fig. 3(A). The PSC device performance is optimized for various dopant concentrations of Cs acetate (0-5 wt%) in ZnO ETL. We have found that PSCs based on 2% cesium acetate doped ZnO ETL demonstrates the most optimum photovoltaic performance. For optimum PSCs along with carbonate ETL as carbonate device we also used 2% cesium carbonate.

The average and best performance of PSCs for both forward bias to short circuit (FB-SC) and short circuit to forward bias (SC-FB) scan directions are listed in Table 2. Ten samples average values have been presented from a random batch. To demonstrate the accurate idea of average PSC performance the best performing devices have not been considered in the

average calculation. Fig. 3(B) shows the current density-voltage (J-V) characteristics of the best performing carbonate and acetate PSCs in both scanning directions. Both the PSCs have some degree of photo-current hysteresis. The average power conversion efficiency of acetate devices is around 15.14% and carbonate devices is around 8.33% which demonstrate about 82% higher average PCE of acetate devices compared to carbonate devices. The PCE of best performing acetate device is 16.45% and carbonate device is 10.01% at FB-SC scan direction which is about 82% higher average PCE in acetate devices. The average open circuit voltage V_{oc} of acetate device is 964.63 mV and carbonate device is 816.39 mV which is nearly 18% higher V_{oc} in acetate devices than carbonate devices. The average short circuit current J_{sc} values are about 6% higher in acetate devices than carbonate devices (acetate: 23.41 mA/cm², carbonate: 22.16 mA/cm²). The average fill-factor FF values are about 45% higher for acetate devices compare to carbonate devices (acetate: 67.07%, carbonate: 46.17%).

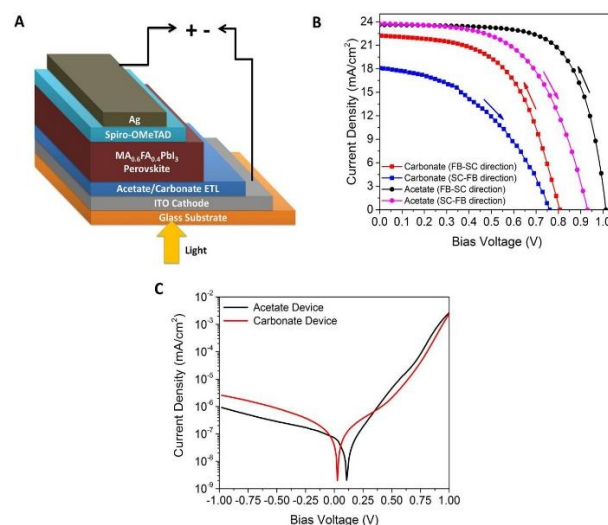


Fig. 3. (A) Schematic diagram of perovskite device structure on acetate and carbonate ETLs; (B) Current density – voltage (J-V) characteristics of perovskite solar cells (both FB-SC and SC-FB direction at 0.05 V/s) of the best performing devices on acetate and carbonate ETLs; (C) Dark J-V curves of PSCs on acetate and carbonate ETLs.

Table 2. Average and best photovoltaic performance of PSCs with acetate and carbonate at both FB-SC and SC-FB directions at a scan rate 0.05 V/s. The average values of ten random samples are listed below with corresponding standard deviation values.

Device	Average/Best	PCE (%)	Short Circuit Current Density, J_{sc} (mA/cm ²)	Open Circuit Voltage, V_{oc} (mV)	Fill Factor, FF (%)	Series Resistance, R_s (Ω .cm ²)	Shunt Resistance R_{sh} (Ω .cm ²)
Carbonate	Average	8.33 ±0.82	22.16 ±0.25	816.39±47.05	46.17 ±4.89	14.76 ±3.13	329±138
	Best (FB-SC)	10.01	22.22	807.02	55.84	9.59	630
	Best (SC-FB)	5.99	18.08	762.01	43.45	14.04	357
Acetate	Average	15.14 ±0.24	23.41 ±0.14	964.63±11.80	67.07 ±1.09	4.72 ±0.40	1145±102
	Best (FB-SC)	16.45	23.61	1012.96	68.79	4.40	1493
	Best (SC-FB)	12.58	23.76	930.47	56.89	8.33	1278

The higher grain sizes in perovskite film on acetate ETL can be related with the increase in V_{OC} compared to carbonate ETL films (**Fig. 2**). In large grain size perovskite film the distance between ionized donor-acceptor pair (DAP) is higher than that in a smaller grain size perovskite film [10]. Higher donor-acceptor distance reduces the acceptor and donor binding energy in the larger grain size perovskite film [10]. The DAP recombination photon energy can be written as [10]:

$$\hbar\omega = E_g - (E_A + E_D) + \frac{q^2}{4\pi\epsilon_0\epsilon_r R} \quad (1)$$

where, E_g , E_A , E_D , q , ϵ_0 , ϵ_r and R are the material bandgap energy, binding energy of acceptor and donor, charge of an electron, dielectric constant of free space, relative dielectric constant of perovskite film and the pair distance of ionized donor-acceptor, respectively. According to Eq. 1, large grain-sized perovskite film on acetate ETL film is anticipated to demonstrate smaller DAP recombination photon energy than that in perovskite layer on carbonate ETL film, owing to higher value of R and smaller magnitudes of E_A and E_D . The higher V_{OC} value of PSC with larger grain sized perovskite film has also been observed in prior studies [5, 13, 36]. The smaller V_{OC} values in carbonate device may be attributed to the heightened surface roughness of perovskite film in it. Rough perovskite surface renders shorting channels [27] to the underneath film and result in current leakage phenomena. The dark current–voltage characteristics were measured for both PSCs devices (acetate and carbonate devices) to understand the leakage current phenomena as shown in **Fig. 3(C)**. The leakage current value in carbonate PSC device is about two times higher than that in acetate PSC device. This observation conforms to our observation of heightened surface roughness of perovskite overlying the carbonate ETL. In dark current-voltage measurement the reverse saturation current density (J_0) is relatively higher in carbonate PSC device than that in acetate PSC device. The open circuit voltage V_{OC} of PSC device can be written as [21]:

$$V_{OC} = \frac{kT}{q} \ln \left(\frac{J_{SC}}{J_0} \right) \quad (2)$$

where, k , T and q are the Boltzmann constant, temperature in kelvin scale and charge of an electron, respectively. According to Eq. 2, observed lower V_{OC} in carbonate PSC device is due to the higher J_0 and lower J_{SC} than acetate devices.

The difference in short circuit current J_{SC} values of two PSC is related with the variation in the n-type property of the two ETLs under study [68]. This is shown in **Fig. 1(B)** from UPS measurements in the difference of Fermi level positions of acetate and carbonate ETLs. The relation between the electron injection barriers between the perovskite conduction

band and the Fermi position of ITO/ETL cathode and the overall J_{SC} values of the PSCs [37, 38] are shown in the band energy diagram, presented in **Fig. 4**. Efficient electron injection from perovskite conduction band at 3.6 eV [38] to cathode ITO/ETL depends on the energetic offset or electron injection barrier between the perovskite conduction band and the Fermi position of ITO/ETL cathode [37, 38]. The electron injection barrier is 0.20 eV in carbonate PSC device, (carbonate PSC in **Fig. 4**). The electron injection barrier value in acetate device (acetate PSC in **Fig. 4**) is 50 meV smaller than carbonate device owing to the reduced work-function in acetate ETL compared to the carbonate ETL. Acetate ETL provides more enhanced electron transfer property [37, 38] in acetate device, with reference to carbonate device because of its lower electron injection barrier (50 meV). Thus, the increased J_{SC} in acetate PSC can be ascribed to the improved electrical conductivity and efficient charge transfer property of acetate ETL film.

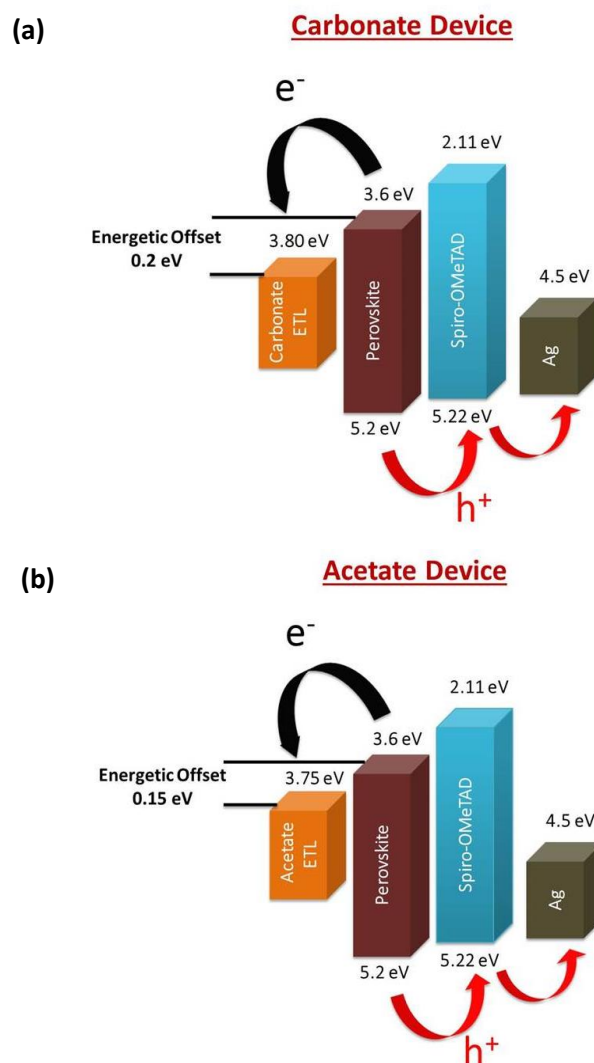


Fig. 4. The energy band diagram of perovskite solar cell structures with (A) carbonate and (B) acetate PSC devices. Carbonate PSC device shows an energetic offset (electron injection barrier) of 0.2 eV between the perovskite LUMO level (3.6 eV) and Fermi position (3.8 eV) of ITO/carbonate ETL contact.

The most enhancements in average PCE of acetate PSC devices come from the improvement in average FF value (45%) in acetate devices, with reference to carbonate devices. In the impedance analysis measurements the average series resistance R_s values in acetate devices is around 3.5 times lower than that in carbonate devices (R_s values - acetate: $4.72 \Omega \cdot \text{cm}^2$, carbonate: $14.76 \Omega \cdot \text{cm}^2$). The average shunt resistance R_{sh} value is around 3.1 times higher in acetate PSC devices than that in carbonate devices (R_{sh} values - acetate: $1145 \Omega \cdot \text{cm}^2$, carbonate: $329 \Omega \cdot \text{cm}^2$). All of these values are listed in **Table 2**.

The observation of larger grain size with reduced grain boundaries in perovskite film on acetate ETL film is consistence with the reduction of series resistance value in acetate PSC devices. In large grain sized perovskite film the reduced number of grain boundaries reduces R_s of a PSC due to enhanced inter-particle connectivity [13]. The lower R_s in acetate PSC device is also connected with the enhanced n-type property of acetate ETL than that in carbonate ETL. Higher R_{sh} value in acetate also conforms to the two-times reduced leakage current J_0 [31] compared to carbonate device (**Fig. 3(C)**).

The flat-band potentials (V_{FB}) are estimated from Mott-Schottky measurements of the fabricated two types of PSCs. The Mott Schottky curves of carbonate and acetate PSC devices are shown in **Fig. 5** under dark at 10 KHz frequency. The calculated V_{FB} in carbonate and acetate devices are 0.83 V and 1.06 V, respectively. The V_{fb} of a PSC can be defined as [23, 51, 52]:

$$V_{fb} = E_{Fn} - E_p \quad (3)$$

where, E_{Fn} and E_p are the fermi level of ETL/cathode and perovskite film, respectively. The difference in V_{fb} values in both acetate and carbonate PSC devices is the difference in work-function [51, 81] in both active layer (perovskite) and ETL films. The smaller grain sized at the perovskite film on carbonate ETL film with larger number of grain boundaries contribute to higher number of recombination-centers for charge carriers compared to acetate ETL [4]. According to Eq. 3 the flat-band potential in carbonate device is decreased due to the enhanced trap-assisted carrier recombination phenomena which elevate the perovskite quasi Fermi level [23], and lower the energetic offset between E_{Fn} and E_p . According to the Mott-Schottky measurements the carrier recombination of acetate devices are significantly low with reference to carbonate devices. This low recombination phenomena lead to improve the FF value and enhanced the device performance with acetate PSC devices.

Photocurrent hysteresis

The current-voltage characteristics of the fabricated PSCs in both FB-SC and SC-FB directions are shown in **Fig. 3(B)**. All the J-V curves of PSCs show some

amount of hysteresis. The hysteresis index (HI) [18, 20, 62] is calculated for both the devices using the following formula:

$$HI = \frac{J_{FB-SC}(V_{OC}/2) - J_{SC-FB}(V_{OC}/2)}{J_{FB-SC}(V_{OC}/2)} \quad (4)$$

where, $J_{FB-SC}(V_{OC}/2)$ and $J_{SC-FB}(V_{OC}/2)$ are the current densities at $(V_{OC}/2)$ in FB-SC and SC-FB directions, respectively. Significantly low HI value is observed in acetate PSCs compared to carbonate PSCs (carbonate device: 0.29, acetate device: 0.03). The HI value is very low [20, 62] in acetate PSC devices. Low HI value in acetate PSC device is consistent for the reduced grain boundary with larger perovskite grain size on acetate ETL [64]. The frequency-dependent capacitive responses of both types of PSC devices are also observed to understand the difference in their hysteretic behaviour. The capacitive responses of carbonate and acetate PSCs under dark at zero external bias are measured as a function of frequency [50, 53, 70]. The capacitive spectra at low frequency region shows significant information about the trap-assisted electrode polarization process [2] in PSCs. Electrode polarization process leads to the photocurrent hysteresis phenomena. Electrode polarization modulate the local electric field in PSC [2] which is related with slow kinetics of migrating ions towards external electrodes [2] of PSCs. Especially at low frequency region in the frequency-dependent capacitive spectra, this phenomenon is demonstrated by large capacitance values [2]. Perovskite solar cells with acetate ETL shows smaller low-frequency (0.1-1 Hz) capacitance compared to carbonate PSCs devices. The low HI values in acetate PSC devices is consistent with reduced value of low-frequency capacitance in acetate devices [2, 35] than that to carbonate PSCs.

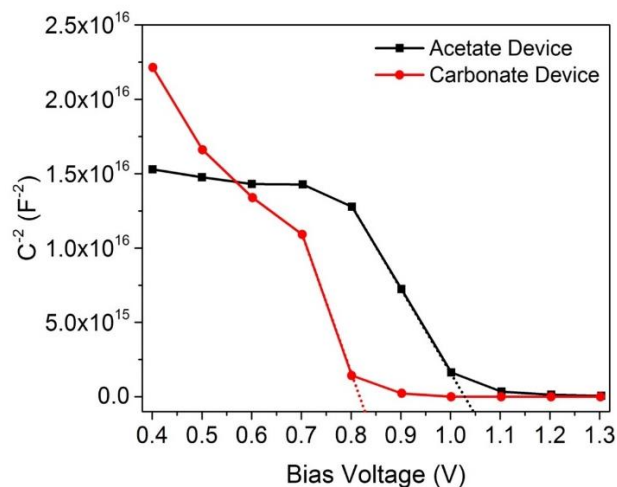


Fig. 5. The plot of capacitance-voltage curves called Mott-Schottky curves of acetate and carbonate devices at 10 KHz frequency under dark condition.

Device stability

The stability of acetate and carbonate PSCs devices was systematically investigated to understand the degradation phenomena [73]. Un-encapsulated PSCs devices were stored for 30 days in a N_2 atmosphere. The device degradation was studied under dark by following the protocols mentioned in previous works [3, 13, 34, 47, 71, 72, 77]. Current-voltage characteristics of PSC devices were measured at every two days intervals at room temperature at a controlled 35% - 40% relative humidity atmosphere. The normalized PCE values of carbonate and acetate PSC devices are shown in Fig. 6(A) from the day of fabrication up to 30 days. The initial values of PCE of acetate PSCs device remain $\sim 87\%$ even after 30 days. The carbonate PSC, PCE drops down to $\sim 21.5\%$ of its commencing efficiency after 30 days.

Normally the grain-boundary in perovskite film are the most chemically active areas [13]. Perovskite atop carbonate ETL has smaller grain with higher number of grain-boundaries has larger chemically active area and lower thermal stability with light-deposited heat during the current-voltage measurements which is also previously reported by Chiang *et al.* [13]. At the carbonate film the melting of smaller perovskite grain leads to the formation of defects or pinholes during the decomposition process in the perovskite film [6, 13], which can decompose it into PbI_2 [6]. The V_{fb} in both aged samples (acetate and carbonate PSC devices) are reduced than to their commencing V_{fb} values (Fig. 6(B) - 6(C)) [23, 51]. Smaller V_{fb} of aged carbonate based PSC suggest towards severe carrier recombination in it [23] than to aged acetate device. The higher intermediate-frequency capacitive values [2, 22, 46] in aged carbonate PSC is also consistent with this observation. In aged carbonate PSC device the higher trap-assisted recombination result in lower normalized PCE values [27, 51] than the aged acetate PSCs.

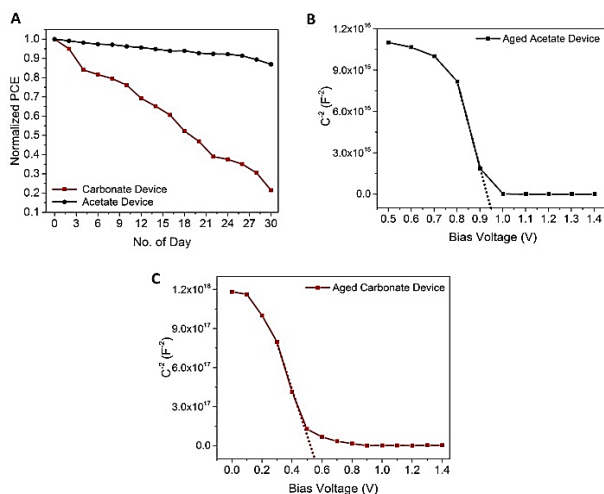


Fig. 6. (A) Normalized PCE of PSCs on acetate and carbonate ETLs as a function of sample storage time in a N_2 filled glove box. Capacitance - voltage curves called Mott-Schottky curves of 1 month old PSCs on (B) acetate ETL and (C) carbonate ETL at 10 KHz frequency under dark condition.

Conclusion

We have systematically investigated and analysed the effects of cesium doped ZnO film for mixed organic cation based $MA_{0.6}FA_{0.4}PbI_3$ PSC in RVSA method. Perovskite overlying the acetate ETL has large and uniform grain distribution, less grain boundaries, pinhole-free. Perovskite solar cells with acetate ETL has less leakage current, smaller contact and larger recombination resistance. PSC device with acetate ETL has higher flat-band potential which leads to the enhanced device performance. The acetate based PSC devices demonstrate nearly 82% higher efficiency with respect to carbonate devices. The best performance acetate based PSC device has PCE 16.45%. The acetate PSC device show low hysteresis phenomena than carbonate devices. Reduced photo-current hysteresis is found to relate with the mitigated electrode polarization phenomena. In the month long degradation studies acetate based PSC devices shows nearly four times higher device stability than carbonate devices. The cesium acetate doped sol-gel ZnO film is a promising ETL for the large-scale manufacturing of efficient and stable perovskite solar cells in roll-to-roll process on flexible substrate.

Acknowledgement

The authors acknowledge the financial support provided by Future Solar Technologies Pty. Ltd. for this work. The authors would like to thank the Australian Centre for Advanced Photovoltaics, SPREE staff and technicians for their kind support. We are also grateful to members in the OPV group for their feedback, helpful discussions and support whilst completing this work.

References

- Ahmedi, M.; Mirabbaszadeh, K.; Salari, S.; Fatehy, H., *Electron. Mater. Lett.*, **2014**, *10*, 951.
- Almora, O.; Zarazua, I.; Mas-Marza, E.; Mora-Sero, I.; Bisquert, J.; Garcia-Belmonte, G., *J. Phys. Chem. Lett.*, **2015**, *6*, 1645.
- Arafat Mahmud, M.; Kumar Elumalai, N.; Baishakhi Upama, M.; Wang, D.; Haque, F.; Wright, M.; Howe Chan, K.; Xu, C.; Uddin, A., *Phys. Status Solidi RRL*, **2016**, *10*, 882.
- Bi, C.; Shao, Y.; Yuan, Y.; Xiao, Z.; Wang, C.; Gao, Y.; Huang, J., *J. Mater. Chem. A*, **2014**, *2*, 18508.
- Bi, C.; Wang, Q.; Shao, Y.; Yuan, Y.; Xiao, Z.; Huang, J., *Nat. Commun.*, **2015**, *6*, 7747.
- Brinkmann, K. O.; Zhao, J.; Pourdavoud, N.; Becker, T.; Hu, T.; Olthof, S.; Meerholz, K.; Hoffmann, L.; Gahlmann, T.; Heiderhoff, R.; Oszajca, M. F.; Luechinger, N. A.; Rogalla, D.; Chen, Y.; Cheng, B.; Riedl, T., *Nat. Commun.*, **2017**, *8*, 13938.
- Burschka, J.; Pellet, N.; Moon, S. J.; Humphry-Baker, R.; Gao, P.; Nazeeruddin, M. K.; Gratzel, M., *Nature*, **2013**, *499*, 316.
- Castelli, I. E.; Garcia-Lastra, J. M.; Thygesen, K. S.; Jacobsen, K. W., *APL Mater.*, **2014**, *2*, 081514.
- Chen, F. C.; Wu, J. L.; Yang, S. S.; Hsieh, K. H.; Chen, W. C., *J. Appl. Phys.*, **2008**, *103*, 103721.
- Chen, J.; Shi, T.; Li, X.; Zhou, B.; Cao, H.; Wang, Y., *Appl. Phys. Lett.*, **2016**, *108*, 053302.
- Chen, Q.; Zhou, H.; Hong, Z.; Luo, S.; Duan, H.-S.; Wang, H. H.; Liu, Y.; Li, G.; Yang, Y., *J. Am. Chem. Soc.*, **2014**, *136*, 622.
- Cheng, Y.; Yang, Q. D.; Xiao, J.; Xue, Q.; Li, H. W.; Guan, Z.; Yip, H. L.; Tsang, S. W., *ACS Appl. Mater. Interfaces*, **2015**, *7*, 19986.
- Chiang, C. H.; Wu, C. G., *ChemSusChem*, **2016**, *9*, 2666.

14. D'Innocenzo, V.; Grancini, G.; Alcocer, M. J. P.; Kandada, A. R. S.; Stranks, S. D.; Lee, M. M.; Lanzani, G.; Snaith, H. J.; Petrozza, A., *Nat Commun*, **2014**, 5.
15. Docampo, P.; Hanusch, F. C.; Stranks, S. D.; Döblinger, M.; Feckl, J. M.; Ehrensperger, M.; Minar, N. K.; Johnston, M. B.; Snaith, H. J.; Bein, T., *Adv. Energy Mater.*, **2014**, 4, n/a.
16. Elumalai, N.; Mahmud, M.; Wang, D.; Uddin, A., *Energies*, **2016**, 9, 861.
17. Elumalai, N. K.; Mahmud, A.; Wang, D.; Wright, M.; Upama, M. B.; Chan, K. H.; Xu, C.; Uddin, A., *43rd IEEE PVSC*, **2016**, 0764.
18. Elumalai, N. K.; Uddin, A., *Sol. Energy Mater. Sol. Cells*, **2016**, 157, 476.
19. Emara, J.; Schnier, T.; Pourdavoud, N.; Riedl, T.; Meerholz, K.; Olthof, S., *Adv. Mater.*, **2016**, 28, 553.
20. Ginting, R. T.; Jung, E. S.; Jeon, M. K.; Jin, W. Y.; Song, M.; Kang, J. W., *Nano Energy*, **2016**, 27, 569.
21. Green, *Englewood Cliffs, NJ, Prentice-Hall, Inc.*, **1982**.
22. Guerrero, A.; Garcia-Belmonte, G.; Mora-Sero, I.; Bisquert, J.; Kang, Y. S.; Jacobsson, T. J.; Correa-Baena, J. P.; Hagfeldt, A., *J. Phys. Chem. C*, **2016**, 120, 8023.
23. Guerrero, A.; You, J.; Aranda, C.; Kang, Y. S.; Garcia-Belmonte, G.; Zhou, H.; Bisquert, J.; Yang, Y., *ACS Nano*, **2016**, 10, 218.
24. Gui-Yang, H.; Chong-Yu, W.; Jian-Tao, W., *J. Phys.: Condens. Matter*, **2009**, 21, 345802.
25. Heo, J. H.; Im, S. H.; Noh, J. H.; Mandal, T. N.; Lim, C.-S.; Chang, J. A.; Lee, Y. H.; Kim, H.-J.; Sarkar, A.; Nazeeruddin Md, K.; Gratzel, M.; Seok, S. I., *Nat Photon*, **2013**, 7, 486.
26. Hu, Q.; Wu, J.; Jiang, C.; Liu, T.; Que, X.; Zhu, R.; Gong, Q., *ACS Nano*, **2014**, 8, 10161.
27. Huang, F.; Dkhissi, Y.; Huang, W.; Xiao, M.; Benesperi, I.; Rubanov, S.; Zhu, Y.; Lin, X.; Jiang, L.; Zhou, Y.; Gray-Weale, A.; Etheridge, J.; McNeill, C. R.; Caruso, R. A.; Bach, U.; Spiccia, L.; Cheng, Y. B., *Nano Energy*, **2014**, 10, 10.
28. Hwang, K.; Jung, Y. S.; Heo, Y. J.; Scholes, F. H.; Watkins, S. E.; Subbiah, J.; Jones, D. J.; Kim, D. Y.; Vak, D., *Adv. Mater.*, **2015**, 27, 1241.
29. Imai, Y.; Watanabe, A., *J. Mater. Sci.: Mater. Electron.*, **15**, 743.
30. Jeon, N. J.; Noh, J. H.; Yang, W. S.; Kim, Y. C.; Ryu, S.; Seo, J.; Seok, S. I., *Nature*, **2015**, 517, 476.
31. Jian-Feng, L.; Chuang, Z.; Heng, Z.; Jun-Feng, T.; Peng, Z.; Chun-Yan, Y.; Yang-Jun, X.; Duo-Wang, F., *Chin. Phys. B*, **2016**, 25, 028402.
32. Jiang, C. S.; Yang, M.; Zhou, Y.; To, B.; Nanayakkara, S. U.; Luther, J. M.; Zhou, W.; Berry, J. J.; van de Lagemaat, J.; Padture, N. P.; Zhu, K.; Al-Jassim, M. M., *Nat Commun*, **2015**, 6, 6.
33. Juarez-Perez, E. J.; Wußler, M.; Fabregat-Santiago, F.; Lakus-Wollny, K.; Mankel, E.; Mayer, T.; Jaegermann, W.; Mora-Sero, I., *J. Phys. Chem. Lett.*, **2014**, 5, 680.
34. Kato, Y.; Ono, L. K.; Lee, M. V.; Wang, S.; Raga, S. R.; Qi, Y., *Advanced Materials Interfaces*, **2015**, 2, n/a.
35. Kim, H. S.; Park, N. G., *J. Phys. Chem. Lett.*, **2014**, 5, 2927.
36. Kim, H. D.; Ohkita, H.; Benten, H.; Ito, S., *Adv. Mater.*, **2016**, 28, 917.
37. Kim, H. P.; Yusoff, A. R. b. M.; Lee, H. J.; Lee, S. J.; Kim, H. M.; Seo, G. J.; Youn, J. H.; Jang, J., *Nanoscale Res. Lett.*, **2014**, 9, 323.
38. Kim, J.; Kim, G.; Kim, T. K.; Kwon, S.; Back, H.; Lee, J.; Lee, S. H.; Kang, H.; Lee, K., *J. Mater. Chem. A*, **2014**, 2, 17291.
39. Kumar, M. H.; Yantara, N.; Dharani, S.; Gratzel, M.; Mhaisalkar, S.; Boix, P. P.; Mathews, N., *Chem. Commun.*, **2013**, 49, 11089.
40. Law, M.; Greene, L. E.; Johnson, J. C.; Saykally, R.; Yang, P., *Nat Mater*, **2005**, 4, 455.
41. Liu, C.; Wang, K.; Du, P.; Meng, T.; Yu, X.; Cheng, S. Z. D.; Gong, X., *ACS Appl. Mater. Interfaces*, **2015**, 7, 1153.
42. Liu, D.; Kelly, T. L., *Nat Photon*, **2014**, 8, 133.
43. Liu, M.; Johnston, M. B.; Snaith, H. J., *Nature*, **2013**, 501, 395.
44. Ma, Z. Q.; Zhao, W. G.; Wang, Y., *Thin Solid Films*, **2007**, 515, 8611.
45. Magne, C.; Moehl, T.; Urien, M.; Gratzel, M.; Pauporte, T., *J. Mater. Chem. A*, **2013**, 1, 2079.
46. Mahmud, M. A.; Elumalai, N. K.; Upama, M. B.; Wang, D.; Chan, K. H.; Wright, M.; Xu, C.; Haque, F.; Uddin, A., *Sol. Energy Mater. Sol. Cells*, **2017**, 159, 251.
47. Mahmud, M. A.; Elumalai, N. K.; Upama, M. B.; Wang, D.; Goncales, V. R.; Wright, M.; Xu, C.; Haque, F.; Uddin, A., *PCCP*, **2017**, 19, 21033.
48. Mahmud, M. A.; Elumalai, N. K.; Upama, M. B.; Wang, D.; Haque, F.; Wright, M.; Xu, C.; Uddin, A., *Sol. Energy Mater. Sol. Cells*, **2017**, 167, 70.
49. Mahmud, M. A.; Elumalai, N. K.; Upama, M. B.; Wang, D.; Puthen-Veetil, B.; Haque, F.; Wright, M.; Xu, C.; Pivrikas, A.; Uddin, A., *Sol. Energy Mater. Sol. Cells*, **2017**, 167, 87.
50. Mahmud, M. A.; Elumalai, N. K.; Upama, M. B.; Wang, D.; Soufiani, A. M.; Wright, M.; Xu, C.; Haque, F.; Uddin, A., *ACS Appl. Mater. Interfaces*, **2017**, 9, 33841.
51. Mahmud, M. A.; Elumalai, N. K.; Upama, M. B.; Wang, D.; Wright, M.; Chan, K. H.; Xu, C.; Haque, F.; Uddin, A., *Electrochim. Acta*, **2016**, 222, 1510.
52. Mahmud, M. A.; Elumalai, N. K.; Upama, M. B.; Wang, D.; Wright, M.; Sun, T.; Xu, C.; Haque, F.; Uddin, A., *RSC Adv.*, **2016**, 6, 86108.
53. Mahmud, M. A.; Elumalai, N. K.; Upama, M. B.; Wang, D.; Zarei, L.; Goncales, V. R.; Wright, M.; Xu, C.; Haque, F.; Uddin, A., *Nanoscale*, **2018**, 10, 773.
54. Major, S.; Banerjee, A.; Chopra, K. L.; Nagpal, K. C., *Thin Solid Films*, **1986**, 143, 19.
55. Manspeaker, C.; Scruggs, P.; Preiss, J.; Lyashenko, D. A.; Zakhidov, A. A., *J. Phys. Chem. C*, **2016**, 120, 6377.
56. Miyata, A.; Mitioglu, A.; Plochocka, P.; Portugall, O.; Wang, J. T.-W.; Stranks, S. D.; Snaith, H. J.; Nicholas, R. J., *Nat Phys*, **2015**, 11, 582.
57. Oh, H.; Krantz, J.; Litzov, I.; Stubhan, T.; Pinna, L.; Brabec, C. J., *Sol. Energy Mater. Sol. Cells*, **2011**, 95, 2194.
58. Pauporté, T.; Jirka, I., *Electrochim. Acta*, **2009**, 54, 7558.
59. Pauporté, T.; Jouanno, E.; Pellé, F.; Viana, B.; Aschehoug, P., *J. Phys. Chem. C*, **2009**, 113, 10422.
60. Pockett, A.; Eperon, G. E.; Peltola, T.; Snaith, H. J.; Walker, A.; Peter, L. M.; Cameron, P. J., *J. Phys. Chem. C*, **2015**, 119, 3456.
61. Ren, Z.; Ng, A.; Shen, Q.; Gokkaya, H. C.; Wang, J.; Yang, L.; Yiu, W. K.; Bai, G.; Djurišić, A. B.; Leung, W. W. F.; Hao, J.; Chan, W. K.; Surya, C., *Scientific Reports*, **2014**, 4, 4.
62. Sanchez, R. S.; Gonzalez-Pedro, V.; Lee, J. W.; Park, N. G.; Kang, Y. S.; Mora-Sero, I.; Bisquert, J., *J. Phys. Chem. Lett.*, **2014**, 5, 2357.
63. Seigo, T.; Hideki, K.; Yoshiji, H.; Hiroshi, O., *Jpn. J. Appl. Phys.*, **1984**, 23, 874.
64. Sheng, R.; Ho-Baillie, A.; Huang, S.; Chen, S.; Wen, X.; Hao, X.; Green, M. A., *J. Phys. Chem. C*, **2015**, 119, 3545.
65. Smirnov, M., *Journal of Advanced Research in Physics*, **2010**, 1.
66. Snaith, H. J.; Abate, A.; Ball, J. M.; Eperon, G. E.; Leijtens, T.; Noel, N. K.; Stranks, S. D.; Wang, J. T.-W.; Wojciechowski, K.; Zhang, W., *J. Phys. Chem. Lett.*, **2014**, 5, 1511.
67. Stranks, S. D.; Eperon, G. E.; Grancini, G.; Menelaou, C.; Alcocer, M. J. P.; Leijtens, T.; Herz, L. M.; Petrozza, A.; Snaith, H. J., *Science*, **2013**, 342, 341.
68. Sun, Y.; Seo, J. H.; Takacs, C. J.; Seifert, J.; Heeger, A. J., *Adv. Mater.*, **2011**, 23, 1679.
69. Uddin, A.; Mahmud, M. A.; Elumalai, N. K.; Wang, D.; Upama, M. B.; Wright, M.; Chan, K. H.; Haque, F.; Xu, C., *Renew. Energy Environ. Sustain.*, **2017**, 2, 7.
70. Upama, M. B.; Elumalai, N. K.; Mahmud, M. A.; Wang, D.; Haque, F.; Goncales, V. R.; Gooding, J. J.; Wright, M.; Xu, C.; Uddin, A., *Org. Electron.*, **2017**, 50, 279.
71. Wang, D.; Chan, K. H.; Elumalai, N. K.; Mahmud, M. A.; Upama, M. B.; Uddin, A.; Pillai, S., *PCCP*, **2017**, 19, 25016.
72. Wang, D.; Elumalai, N. K.; Mahmud, M. A.; Wright, M.; Upama, M. B.; Chan, K. H.; Xu, C.; Haque, F.; Conibeer, G.; Uddin, A., *Org. Electron.*, **2018**, 53, 66.
73. Wang, D.; Wright, M.; Elumalai, N. K.; Uddin, A., *Sol. Energy Mater. Sol. Cells*, **2016**, 147, 255.
74. Wang, Q.; Shao, Y.; Dong, Q.; Xiao, Z.; Yuan, Y.; Huang, J., *Energy Environ. Sci.*, **2014**, 7, 2359.
75. Wehrenfennig, C.; Eperon, G. E.; Johnston, M. B.; Snaith, H. J.; Herz, L. M., *Adv. Mater.*, **2014**, 26, 1584.

76. Wojciechowski, K.; Stranks, S. D.; Abate, A.; Sadoughi, G.; Sadhanala, A.; Kopidakis, N.; Rumbles, G.; Li, C.-Z.; Friend, R. H.; Jen, A. K. Y.; Snaith, H. J., *ACS Nano*, **2014**, *8*, 12701.
77. Wu, C. G.; Chiang, C. H.; Tseng, Z. L.; Nazeeruddin, M. K.; Hagfeldt, A.; Gratzel, M., *Energy Environ. Sci.*, **2015**, *8*, 2725.
78. Wu, C. I.; Lin, C. T.; Chen, Y. H.; Chen, M. H.; Lu, Y. J.; Wu, C. C., *Appl. Phys. Lett.*, **2006**, *88*, 152104.
79. Xiao, M.; Huang, F.; Huang, W.; Dkhissi, Y.; Zhu, Y.; Etheridge, J.; Gray-Weale, A.; Bach, U.; Cheng, Y. B.; Spiccia, L., *Angew. Chem.*, **2014**, *126*, 10056.
80. Yang, J.; Siempelkamp, B. D.; Mosconi, E.; De Angelis, F.; Kelly, T. L., *Chem. Mater.*, **2015**, *27*, 4229.
81. Yang, W.; Yao, Y.; Wu, C. Q., *J. Appl. Phys.*, **2015**, *117*, 095502.
82. Ye, T.; Petrović, M.; Peng, S.; Yoong, J. L. K.; Vijila, C.; Ramakrishna, S., *ACS Appl. Mater. Interfaces*, **2017**, *9*, 2358.
83. You, J.; Yang, Y.; Hong, Z.; Song, T. B.; Meng, L.; Liu, Y.; Jiang, C.; Zhou, H.; Chang, W. H.; Li, G.; Yang, Y., *Appl. Phys. Lett.*, **2014**, *105*, 183902.
84. Zhang, J.; Pauporté, T., *J. Phys. Chem. C*, **2015**, *119*, 14919.
85. Zhao, X.; Shen, H.; Zhang, Y.; Li, X.; Zhao, X.; Tai, M.; Li, J.; Li, J.; Li, X.; Lin, H., *ACS Applied Materials & Interfaces*, **2016**, *8*, 7826.
86. Zheng, Z.; Lu, Y. F.; Ye, Z. Z.; He, H. P.; Zhao, B. H., *Mater. Sci. Semicond. Process.*, **2013**, *16*, 647.
87. Zhou, H.; Chen, Q.; Li, G.; Luo, S.; Song, T.-b.; Duan, H.-S.; Hong, Z.; You, J.; Liu, Y.; Yang, Y., *Science*, **2014**, *345*, 542.
88. Znaidi, L., *Mater. Sci. Eng. B*, **2010**, *174*, 18.